Chinese Journal of Aeronautics 28 (2015) xx-xx

Contents lists available at ScienceDirect

Chinese Journal of Aeronautics

journal homepage: www.elsevier.com/locate/cja

Deep Learning Enabled Localization for UAV Autolanding

Abstract

This article concentrates on ground vision guided autonomous landing of a fixed-wing Unmanned Aerial Vehicle (UAV) within Global Navigation Satellite System (GNSS) denied environments. Cascaded deep learning models are developed and employed into image detection and its accuracy promoting for UAV autolanding, respectively. Firstly, we design a target bounding box detection network *BboxLocate-Net* to extract its image coordinate of the flying object. Secondly, the detected coordinate is fused into spatial localization with an extended Kalman filter estimator. Thirdly, a point regression network *PointRefine-Net* is developed for promoting detection accuracy once the flying vehicle's motion continuity is checked unacceptable. The proposed approach definitely accomplishes the closed-loop mutual inspection of spatial positioning and image detection, and automatically improves the inaccurate coordinates within a certain range. Experimental results demonstrate and verify that our method outperforms the previous works in terms of accuracy, robustness and real-time criterions. Specifically, the newly developed *Bbox-Locate-Net* attaches over 500 fps, almost five times of the published state-of-the-art in this field, with comparably localization accuracy.

Keywords: UAV autolanding; Ground Vision; Safe landing; Deep Learning; Spatial Localization

*Corresponding author. Tel.: +86 20 xxxxxxxx.
E-mail address: xxxx@xxx.edu.cn

1. Introduction

In the past few decades, unmanned aerial vehicles (UAVs) have drawn more and more attention from many pragmatic fields because of its remarkable characteristics, such as low risk of casualties, low cost, lightweight, and great mobility associated with adaptability to dirty, dull and/or dangerous situations. UAVs have demonstrated their usefulness in a variety of practical applications of meteorological detection, local area monitoring, survey and mapping, forest fire prevention, earthquake rescue[1] and so on. With the integration of advanced automation technology, unmanned vehicles can perform regular-cruise tasks with quite little manual intervention, since the task workspace is almost wide when the vehicle is flying in the air. However, take-off and/or landing is still a technological challenge because the vehicle works in a quite compact space that has complicated relationship with the ground. Specifically, landing of the fixed-wing vehicles has been proved to be the most challenging and hazardous period of aerial flight in many practical applications.[2] Even minor errors in guidance or control might cause system damages or even crashes. This situation becomes more remarkable due to a variety of complex application scenarios and meteorological environment conditions. Under such circumstances, autonomous landing has been an important and essential technique for unmanned systems within unknown or Global Navigation Satellite System (GNSS)-denied scenarios.[3] Hereafter, autonomous landing within GNSS-denied scenarios is called as autolanding. Furthermore, this article concentrates on vision-based localization for autolanding then.

Previous research on vision-based autonomous UAV landing can be categorized into onboard vision and ground vision modes. The onboard vision mode usually employs one or more cameras installed on the flying vehicle as a positioning sensor.[4,5,6] When the aerial vehicle approaches the ground runway, the camera detects the runway and plans an appropriate landing trajectory. In contrast, the ground vision mode distributes and fixes vision systems on the ground.[7,8,9]

Compared with onboard navigators, the ground vision system possesses more scalable computing resources and can save costs by placing them on a runway instead of configuring each vehicle separately. Furthermore, the image from the ground-to-air perspective is much more convenient for processing, than the images from the air-to-ground view. Therefore, in this study, we focus on the ground vision mode for autolanding of fixed-wing unmanned aircrafts.

In the past few years, several prototypes of ground vision based autonomous landing systems have been developed in [7-9], respectively. All are concerned with a mapping from image sequence to spatial trajectory by using computer vision which usually involves two workflow steps: flying vehicle target detection and automatic positioning. In this study, the vision automatic detection schemes are concerned and considered further. As for similar scenarios, Yang et al.[7] presented accurate UAV landing performance in a GPS denied-environment, by running a ground-based near infrared camera system. A nose infrared laser lamp is fixed on the vehicle as a cooperative marker for image detection. The foreground area of the candidate targets is obtained by a simple morphological pre-processing. Researchers at Portuguese Navy Research Center[8] used a ground based monocular vision system supporting the autonomous landing of a fixed-wing aerial vehicle onto a fast patrol boat. For obtaining the relative pose of the vehicle, they have used several 3D model-based system combinations using the Computer-Aided Design (CAD) model for tracking. Both systems need to know the geometrical model or place the cooperative marker on the flying vehicle. On the contrary, Kong and Hu developed a traditional stereo ground-based system including two pan-tilt units and two cameras, without relying on any cooperative onboard markers or geometrical knowledge.[9] Since the system was conducted, Hu, Tang, Cao et al.[3,9,11] have been working on algorithms of automatic detection and localization on an autolanding vehicle. Both corner-based and skeleton-based algorithms have been designed and implemented to target detection on the ground captured sequential images.[3,12] Tang, Hu et al. [3] initially integrated the active contour method into Chan-Vese model detection, and an extended Kalman estimator was developed for ground vision based localization. Thanks to on-ground sufficient computing resources, Cao et al.[13] adopted and improved a flying vehicle tracking algorithm based on GOTURN, which attaches the frame rate to 100 fps, nearly 5 times higher than that of the Chan-Vese algorithm.

Although the pre-existing researches have shown remarkable detection performance in the UAV autolanding processing, challenges still exist in accuracy, robustness and real-time feature, respectively. Yang's target detection method[7] is only suitable for UAVs equipped with infrared laser lamp at the nose, which is difficult to be generalized for various types of aerial crafts. Due to the processing rate of below 25 fps, the real-time performance of Chan-Vese is seldom appropriate for practical applications of autolanding.[3] Similarly, the GOTURN tracking based method[13] relies on human-computer interaction for labeling the bounding box within the first frame. Meanwhile, the tracking error ought to accumulate for a long-term period. Once a frame is tracked to the fall target, it may cause inefficacy of the whole vision-based tracking even. Particularly, some scenarios cannot be correctly treated by using the pre-existing methods. For instance, part of the landing vehicle goes out of the field of view, and only the partial body is captured from the images.

Under such circumstances, this paper innovatively employs deep learning into mapping sequential image frames into spatial localization during the fixed-wing aircraft's autolanding. Deep learning supports a higher processing speed of target detection, and enables a greater accuracy promotion of vision-based positioning further. The overall algorithm has a great improvement in accuracy, robustness and real-time than the previous works. The contributions of this paper are summarized as follows:

(1) A light-weight convolutional deep neural network model, namely *BboxLocate-Net*, is proposed and implemented to perform an initial coarse prediction on spatial coordinates of the landing aircraft. The proposed *BboxLocate-Net* solves the problem that the too-many-parameters-tuning of the classic object detection deep network and achieves a practical and effective balance between speed and accuracy.

(2) A spatial motion continuity criterion is defined and fused into quantitative checking on the landing target detection, by taking full advantage of the high-speed rate of the light-weight detection network.

(3) A key point regression network, namely *PointRefine-Net*, is developed to promote localization accuracy once the flying vehicle's motion continuity is checked unacceptable. Then, the self-correction of error detection is realized, and both robustness and accuracy are improved simultaneously.

2. Ground vision for UAV autolanding

Aiming at runway taxiing and landing of medium aerial vehicles, a ground stereo vision-based system has been developed and updated for several times.[3,9,14,15] Previous several corresponding mapping algorithms to produce the spatial trajectory of the landing vehicle has also completed several online experiments supported by the on-ground vision system.[3,9,12,13] Here, the ground vision system deployment and overall workflow for the ground-to-air visual system is reviewed and presented.

2.1 System architecture and deployment

The ground stereo vision-based system usually works in the aircraft descending and taxing stages to guide it moving in the field of view to accomplish automatic landing. It usually consists of four modules: image capture module, target detection module, position calculation module and data transmission module.[3,9] In the image capture module, two binocular cameras are symmetrically installed on the independent Pan-Tilt units (PTUs) to capture the landing sequential images. Each PTU with camera module works independently and has two degrees of freedom to expand the search scope. Each PTU is controlled and serves to track the landing target and feeds the pitching and yawing angles backward. The target detection module and position calculation module are used for 2D image target detection and 3D spatial location calculation, respectively. Both of them run on the same ground image processing computer. The data transmission module transmits the calculated spatial coordinates onto the onboard autopilot via wireless data link. A general deployment scheme has been designed and implemented for ground stereo guidance prototypes, as shown in Fig. 1.

In real-scenario flights, a fixed-wing unmanned aircraft is guided into the view of the stereo camera by its onboard navigation system. Once the target is detected, the ground-based guidance system switches from the waiting state to the working mode. Two cameras capture the vehicle landing images, and then, the captured sequential images and PTU parameters are transferred to the image processing computer which detects the key point of the flight target and calculates its spatial coordinates. Finally, the spatial coordinates are wirelessly transmitted onto the onboard autopilot to facilitate autonomous landing.

In terms of deployment details, we assume that the origin of the world coordinate system (X, Y, Z) is at the rotation center of the left PTU, from the practical viewpoint of the published works [3,9,13]. The axis of the camera frame is parallel to that of the PTU frame in the initial position. The right camera is mounted on the X-axis, with the light center of the left and right cameras represented as O_l and O_r, respectively. The baseline of the optical system is O_lO_r. θ_l, θ_r, α_l and α_r respectively represent the tilt and pan angles. The anticlockwise measurement is positive. At the same time, the hardware configuration is updated to be compatible with the deep learning requirements. The captured image is transferred to the high-performance computing platform instead of the original control computer. The GPU component performs high-load computations for flight target detection in sequential images, while the CPU is responsible for information-based positioning and wireless data transmission.

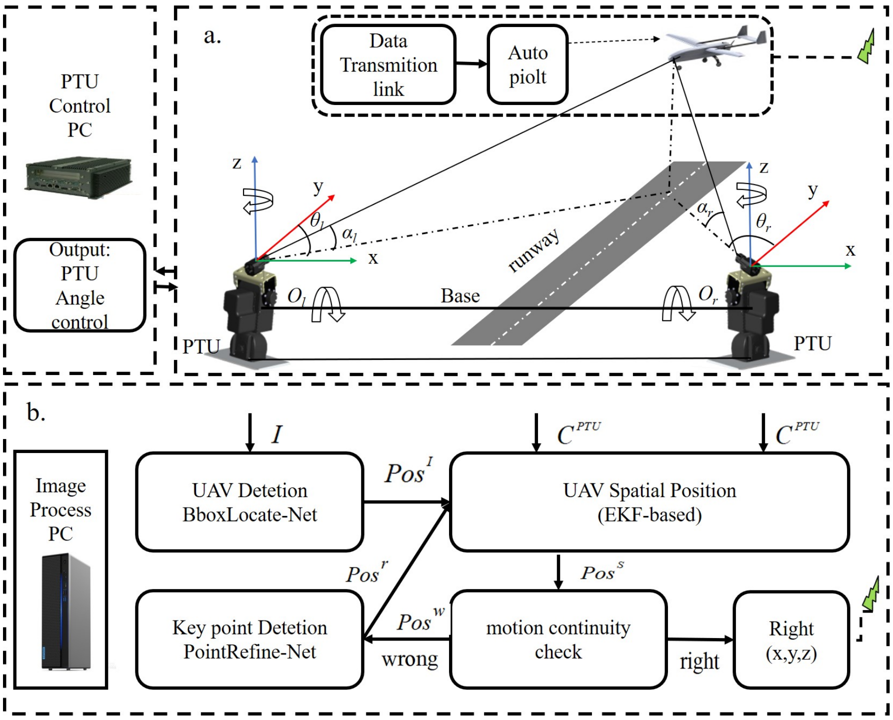

Fig. 1. Schematic diagram of the ground stereo system for autonomous landing of the fixed-wing aerial vehicle. (a) General configuration and deployment of the developed ground vision system; (b) Overall workflow of the developed algorithm models from sequential images into spatial trajectory.

2.2 Overall workflow of vision-based localization

The ground stereo vision-based location algorithm outputs the aircraft spatial coordinates during its autolanding process, while captured sequential images and camera attitudes are inputted online. Generally speaking, the overall workflow is composed of image-based target detection and filter-based localization.

On the basis of the system described in Section 2.1, the previous positioning algorithms have been developed and verified within simulation and experimental scenarios.[3] The landing vehicle's spatial coordinates are directly mapped by using the stereo measurement model, once knowing the target coordinates of the left as well as right images and the PTU attitude parameters. In details, it assumes that the UAV actual coordinate is (x_w, y_w, z_w), and its coordinate on the left and right image plane is (u_l, v_l) and (u_r, v_r), respectively. f is the focal length of the camera. R^L and R^R represent the rotation matrix of the world coordinate system relative to the left and right camera coordinate systems respectively. Then, the relationship of the coordinate between the 3D world and 2D image plane is calculated by:

$$\begin{bmatrix} u_l \\ v_l \\ 1 \end{bmatrix} = \frac{1}{z_c} \cdot \begin{bmatrix} f/d_x & 0 & u_0 & 0 \\ 0 & f/d_x & v_0 & 0 \\ 0 & 0 & 1 & 0 \end{bmatrix} \begin{bmatrix} R^L & T^L \\ 0^T & 1 \end{bmatrix} \begin{bmatrix} x_w \\ y_w \\ z_w \\ 1 \end{bmatrix} \tag{1}$$

$$\begin{bmatrix} u_l \\ v_l \\ 1 \end{bmatrix} = \frac{1}{z_c} \cdot \begin{bmatrix} f/d_x & 0 & u_0 & 0 \\ 0 & f/d_x & v_0 & 0 \\ 0 & 0 & 1 & 0 \end{bmatrix} \begin{bmatrix} R^L & T^L \\ 0^T & 1 \end{bmatrix} \begin{bmatrix} x_w \\ y_w \\ z_w \\ 1 \end{bmatrix} \tag{2}$$

$$\begin{cases} u_l = f_{ul}\left(x_w, y_w, z_w, \alpha_l, \theta_l\right) \\ v_l = f_{vl}\left(x_w, y_w, z_w, \alpha_l, \theta_l\right) \\ u_r = f_{tr}\left(x_w, y_w, z_w, \alpha_r, \theta_r\right) \\ v_r = f_{vr}\left(x_w, y_w, z_w, \alpha_r, \theta_r\right) \end{cases} \tag{3}$$

The stereo vision algorithm processes the spatial coordinates one point by one point, so random disturbance is inevitably involved in the outputted trajectory under the mentioned principle of triangulation. Tang and Hu et al.[3] proposed an extended Kalman filter estimator to improve localization accuracy by fusing knowledge of aircraft motion continuity. Here, X= (x_w, y_w, z_w, v_x, v_y, v_z) ^{T} denotes state variables, Y= (u_l, v_l, u_r, v_r) ^{T} means the observation values of detected target coordinates in images. By constructing the state observation equation Eq. (4) and the state estimation equation Eq. (5), the whole system state estimation process is completed through five recursive steps of extended Kalman filter. Real-scenario flight experiments have demonstrated that this method is more robust and accurate than the triangulation-based localization algorithm.[3]

$$\begin{gathered} \hat{X}_{(k|k-1)} = F\hat{X}_{(k-1|k-1)} + \Gamma W_k \\ \hat{Y}_{(k-1|k-1)} = h_k\left(\hat{X}_{(k-1|k-1)}\right) + V_k \end{gathered} \tag{4}$$

$$Y_{(k|k-1)} = h_k\left(\hat{X}_{(k-1|k-1)}\right) = \begin{bmatrix} u_l \\ v_l \\ u_r \\ v_r \end{bmatrix} = \begin{bmatrix} f_{ul}\left(x_w, y_w, z_w, v_x v_y, v_z\right) \\ f_{vl}\left(x_w, y_w, z_w, v_x, v_y, v_z\right) \\ f_{ur}\left(x_w, y_w, z_w, v_x, v_y, v_z\right) \\ f_{v}\left(x_w, y_w, z_w, v_x, v_y, v_z\right) \end{bmatrix} \tag{5}$$

Eventually, this article employs deep learning models into a fast and accurate detection on the autolanding sequential images, since the pre-existing works need to be promoted with the processing rate and localization accuracy. Specifically, the proposed approach will be an original trial for the challenging scenario when the landing aircraft is partially out of the field of view.

3. Deep learning models enabling accurate and fast detection

In this study, a cascaded deep learning model is proposed and developed to enable ground vision based autolanding, with considerations on the existing challenges of real-time and accuracy. Such a scheme takes full advantage of the scalability of computing resources supported by the ground vision system. Firstly, the ground stereo mode is flexibly extendable to computing and/or storage resources. Here, we upgrade the computing platform to GTX1080ti to run the deep learning algorithm more efficiently. Secondly, annotated mixed landing datasets are conducted through a large number of actual and simulation flight experiments. Hereafter, two lightweight learning networks are developed to enable a fast and accurate detection on the autolanding vehicle. Such a hierarchical structure processes vision-based localization from coarse extraction to fine correction. Thirdly, the system scalability is both feasible and effective for improving the real-time and accuracy of the ground stereo guidance system. Finally, higher processing speed provides extra operations of motion continuity checking and coordinate correction for autolanding localization. Furthermore, the proposed two-hierarchy deep neural models are implemented, demonstrated and validated as well.

3.1. Two-hierarchy architecture of cascaded deep neural networks

A cascade two-hierarchy convolution networks is employed to make fast coarse-to-fine prediction. In the first hierarchy, we propose a bounding box regression-based convolutional network, whose input is the complete image captured by the camera. It is mainly responsible for predicting the aircraft ROI (region-of-interest) coordinates in the whole image, and assuming the center point of the bounding box as the key point location. The second hierarchy network takes the local ROI predicted by the first-hierarchy network as input, allowing only a certain range of modifications to the former coarse predictions. The inputted image size and search range keep decreasing along the cascade.

The detected bounding box certainly contains or covers the landing aircraft, but mismatching does exist between the detected box's center and the actual image coordinates in either horizontal or vertical direction. Such mismatching phenomenon often results in localization inaccuracy of the landing vehicle. It is even worse to lead to failure of the visual positioning task. Hereafter, we introduce a second-level network to optimize the accuracy of the vision-based localization algorithm. Under such two-hierarchy architecture, the first level aims to estimate key point position robustly with few considerable errors, while the second level is designed to produce higher accuracy.

The proposed cascaded deep learning detection method consists of four stages, as shown in Fig.2. In details, *BboxLocate-Net* represents the first-level network, and *PointRefine-Net* represents the second-level network. In the first stage, an autolanding image dataset with annotations is conducted to train the coarse detection model *BboxLocate-Net*. It is followed by a *PointRefine-Net* training process which takes lots of random small areas including key points as samples. In the third stage, the captured UAV image is detected by *BboxLocate-Net*. In the fourth stage, the bounding box produced by the *BboxLocate-Net* detection module is finally used by the point refinement module *PointRefine-Net* to obtain a more accurate estimation of the guiding target.

In the following sub-section 3.2 and 3.3, we focus on the deep neural network structure and algorithm workflow of each hierarchy. The combining strategies of cascade two-level networks are to be presented in sub-section 3.4.

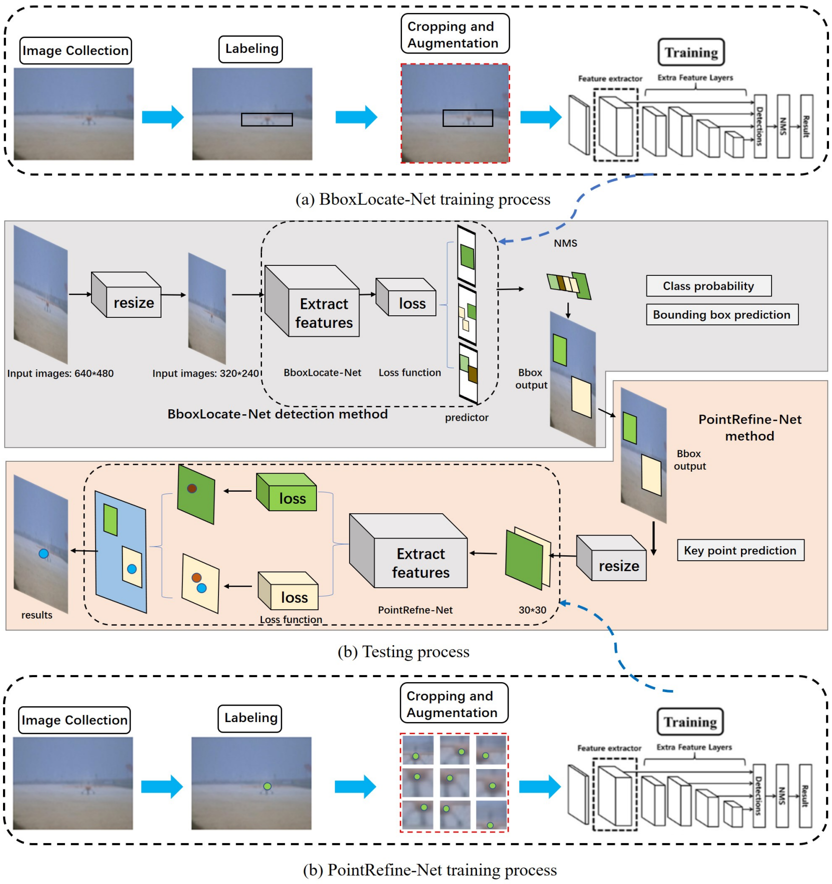

Fig. 2. Structure of the detection model based on the *BboxLocate-Net* and *PointRefine-Net*. (a) *BboxLocate-Net* training pro cess; (b) Testing process; (c)*PointRefine-Net* training process.

3.2. Deep learning based target detection

The goal of detection algorithm is to locate and classify the targets during the UAV autolanding process. The detected objects are usually labeled with bounding boxes, category information and confidence score as well.

Recently, there have been more and more researches on object detection. Faster R-CNN, [19] the two-stage proposal-driven CNN object detector, reaches great accuracy on many challenging datasets, while the processing speed is still a major concern. Facts show that it is obvious that Faster R-CNN is not an optimal solution for real-time flying vehicle detection. YOLO v3, [20] the one-stage detector, not only demonstrates promising results but also yields about 10 times faster detection speed. Experimental results demonstrate its accuracy reduced by about 12% compared to Faster R-CNN, and it still can hardly achieve real-time detection in the autolanding scenarios.

Considering the balance between accuracy and processing time, this paper proposes a novel UAV object detection network named *BboxLocate-Net* which is designed to create a smaller-scale, faster, and more efficient deep neural model. Neither increasing the network depth nor width, we deal with the problem from another perspective. Using DenseNet[21] for reference, we exploit the potential of the network through feature reuse and multi-scale fusion. We combine *BboxLocate-Net* as the feature extractor and YOLOv3 predictor. The *BboxLocate-Net* algorithm training and testing process are shown in Fig.2.

We design *BboxLocate-Net*'s architecture based on the several principles of improving the real-time capacity and accuracy simultaneously. At first, reducing the network parameters is the key to improve the real-time performance. It is inspired by the DenseNet[21] network to enhance the feature reuse between layers, full use shallow and deep information, and reduce the number of parameters. The proposed network introduces a dense connection from one layer to all subsequent layers, developing a highly dense feature reuse connection among the five-layer feature maps. Different from DenseNet, we cascade the feature maps as the decreasing order of their resolution. In this study, it is named as "Ladder-Dense" connection.

Then, the network is further designed to improve the detection accuracy. When the landing vehicle approaches and descends, the target is usually small and the background is relatively complex. The small target in the deep low-resolution feature map is usually apt to be lost. Since it makes worse accuracy of small-scale target detection, an HRNet[22] inspired approach is adopted to make full use of the information across all scales of the image, and reduce the loss of feature maps information due to the decrease of image resolution. Such a HRNet-inspired network works with a high-resolution subnetwork as the first parallel path, and gradually adds the other low-resolution layer's resolution-hold parallel path one by one. As a result, the parallel path explores the network potential while maintaining resolution. In the output part of the network, a multi-scales fusion unit is deployed to cascade the information from all parallel subnetworks[21] to capture and integrate information at all scales of an image.

Finally, considering the real-time and accuracy of the detection network, the proposed *BboxLocate-Net* is tested with excellent performance in specified datasets. It has been noted that HRNet and DenseNet, two state-of-the-arts networks, have produced excellent performance in large-scale dataset detection tasks such as COCO[23] and ImageNet[24]. Specifically, the autolanding image datasets have only two classes of plane and background. The proposed *BboxLocate-Net* rightly achieves a balance between prediction accuracy and processing speed, by combining the advantages of Densenet and HRNet together.

During the detection process, each image captured from the ground cameras is resized to 320×240 to match *BboxLocate-Net*. Then, the 20×15×18 prediction tensor is automatically generated through the feature extraction network *BboxLocate-Net* and the YOLO detection layer. Each of the 1×1×30 tensor includes the target location information: center coordinates (x, y), width w, height h, category information and confidence score c.[20] After obtaining the confidence c of each prediction box, a threshold will be set to remove the boxes with a score below. Then the remaining bounding boxes are filtered with the non-maximal suppression to obtain multiple sets of high-score bounding boxes. In particular, the YOLOv3 predictor uses a set of initial anchor boxes with fixed width and height to regress and predict the target position. Here, K-means clustering[25] is adopted to determine the number and the best size of anchor boxes. As shown in Fig.3, three clustering centers are presented for the training dataset using K-means clustering. The yellow box and the blue box respectively represent two benchmark anchor boxes with different sizes. The final red box predicted by *BboxLocate-Net* is calculated based on three anchor boxes.

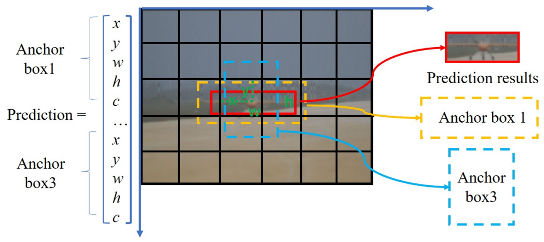

Fig. 3. Detection results based on multiple anchor boxes. The yellow box and blue box respectively represent two benchmark anchor boxes of different sizes. The Red box is the prediction result.

The kernel task of the *BboxLocate-Net* network is to calculate the object confidence value, while prediction on the width, height and central coordinates of the UAV target is concerned as well. For example, *Loss* values of aircraft detection generally include head frame coordinate loss $Loss_{coor}$ and confidence loss $Loss_{conf}$. The calculation equation is as follows:

$$Loss(UAV) = Loss_{coor} + Loss_{conf} \tag{6}$$

On one hand, $Loss_{coor}$ is quantitatively analyzed by

$$\begin{aligned} Loss_{coor} = \lambda_{coord} \sum_{i=0}^{S^2} \sum_{j=0}^{B} I_{ij}^{obj} \left[\left(x_i - \hat{x}_i \right)^2 + \left(y_i - \hat{y}_i \right)^2 \right] + \\ \lambda_{coord} \sum_{i=0}^{S^2} \sum_{j=0}^{B} I_{ij}^{obj} \left[\left(\sqrt{w_i} - \sqrt{\hat{w}_i} \right)^2 + \left(\sqrt{h_i} - \sqrt{\hat{h}_i} \right)^2 \right] \end{aligned} \tag{7}$$

where I_{ij}^{obj} denotes the possibility of a landing target in the j th anchor box of the i th grid; λ_{coord} is the weight of positioning error, generally equal to 5; x_i, y_i, w_i, and h_i represent the UAV bounding box coordinates, width and height which is detected in i th grid, respectively. $\hat{x}_i$, $\hat{y}_i$, $\hat{w}_i$ and $\hat{h}_i$ mean actual position parameters from training data of the i th grid. S^2 represents the total number of grids after passing through the network. B is the number of anchor boxes.

On the other hand, the loss function of confidence $Loss_{conf}$ is quantified as

$$Loss_{conf}=\sum_{i=0}^{S^2}\sum_{j=0}^{B}I_{ij}^{obj}\left[\left(C_i-\hat{C}_i\right)^2\right]+\lambda_{noobj}\sum_{i=0}^{S^2}\sum_{j=0}^{B}I_{ij}^{noobj}\left[\left(C_i-\hat{C}_i\right)^2\right] \tag{8}$$

where λ_{noobj} denotes the weight coefficient of confidence error. C_i indicates the confidence of the target contained in the i th grid of all S^2 grids. $\hat{C}_i$ represents the confidence parameter of the i th grid in the manually labeled data.

3.3. Deep learning based accuracy promoting

In the previous works of ground vision based autolanding, the sequential coordinates are directly calculated once the detection is done, because its detection frame rate just satisfied the fundamental requirement of autolanding [3,13]. There is no extra time for correction or refinement if the detection inaccuracy occurs or even cumulates. Therefore, we propose a second level point regression network to further optimize the target's image coordinates. The above mentioned *BboxLocate-Net* greatly optimizes the speed of UAV target detection and provides the possibility for the implementation of motion continuity check and coordinate correction.

For practical applications, a criterion for checking the motion continuity is definitely in need to trigger whether or not to conduct an accuracy promoting algorithm. In this paper, we synthesize the distance and angle indexes into the motion continuity criterion. We define F (x_i, y_i) as the candidate point. P (x_1, y_1) and Q (x_2, y_2) denote the last two points of flying trajectory, $|FQ|$ denotes the space distance between point F and point Q. Then when the following two conditions are satisfied at the same time, F is regarded as correct. Otherwise, it is confirmed to be mismatched and has to be corrected then.

$$|FQ|=\sqrt{(x_i-x_2)^2+(y_i-y_2)^2+(z_i-z_2)^2}\le 1.5|PQ| \tag{9}$$

$$\angle PQF \ge 120^{\circ} \tag{10}$$

Then, once the output of the first-level network is checked as not acceptably continuous, the second-level point regression network *PointRefine-Net* starts to run. *PointRefine-Net* is a key point regression network which is responsible for correcting the key point coordinates in a small ROI. The training samples are 9 small areas with different sizes and positions randomly captured near the key points of each picture. The network is mainly for optimizing the offset value (x, y) of the key point from the upper left corner of the area. In order to minimize the loss of key point coordinate offset, the convolution kernel parameters are updated iteratively by using the backward gradient propagation algorithm. When the loss value is less than the threshold value 0.002, the network stops training and we get the final point regression network model. Fig. 2 (c) shows the training process of *PointRefine-Net*.

We also design *PointRefine-Net*'s architecture based on the several principles of improving the real-time capacity and accuracy. Since the input of the second level network is only a small part of the original image, we design a resolution preserving point regression network. The feature extraction network is basically the same as the sequential path part of *BboxLocate-Net*. However, the difference between of them is that the resolution of the first few layer changes from high to low in *BboxLocate-Net* but stays the same in *PointRefine-Net*. In the shallow layers, for encouraging feature reuse, the front layer of feature extraction network of *PointRefine-Net* uses dense connection. In the deep layers, to effectively process and consolidate features across scales, we choose to use a single pipeline with skip layers to preserve spatial information at each resolution which is proposed in Hourglass. [26]

Finally, the first five layers of *PointRefine-Net* are connected with Dense-connection, and the output part with Hourglass-connection[26]. Based on the structure, *PointRefine-Net* becomes a simple, minimal deep learning detection network that has the capacity to capture all of these features and bring them together to output pixel-wise predictions.

In the process of key point detection, the input of *PointRefine-Net* is an inaccurate bounding box containing UAV target detected by *BboxLocate-Net* network. After the image resolution is resized to *30* × *30*, the convolution operation is carried out. The output tensor only contains the key point coordinate information (x, y). Fig.4 shows the optimization process of *PointRefine-Net* from the inaccurate bounding box detected by *BboxLocate-Net* to the accurate point.

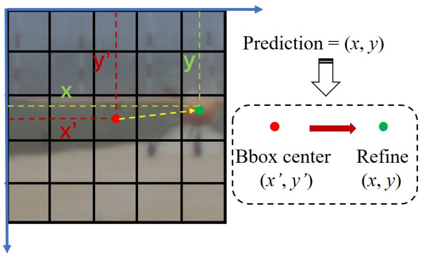

Fig. 4. Schematic diagram of error coordinate correction. The red dot is a wrong detection result. The green dot indicates the corrected result.

The only task of *PointRefine-Net* network is to predict the key point coordinate vector. For a UAV head key point, Eq. (11) is the loss function of the head key point regression task.

$$Loss = \sum_{i=0}^{S^2}\sum_{j=0}^{B} I_{ij}^{obj}\left[(x_i-\hat{x}_i)^2+(y_i-\hat{y}_i)^2\right] \tag{11}$$

where x_i and y_i represent the center coordinates of the predicted i th grid. $\hat{x}_i$ and $\hat{y}_i$ stand for actual position parameters from training data of the i th grid.

3.4. Vision-based localization algorithm and workf low

Combining with sub-section 2.2 and the detailed description of the cascaded detection models, we present our overall location algorithm flow chart. When actually detecting the UAV target, first, the *BboxLocate-Net* network receives the complete image and predicts the bounding box coordinate of the UAV target. Then, combining with PTUs parameters, we calculate the UAV spatial position based on EKF-based object spatial localization algorithm[3] and check the motion continuity. If the coordinate is checked as an error point, we take the local ROI pre-dicted by the *BboxLocate-Net* as the input of second level network. Finally, *PointRefine-Net* can precisely correct the key point coordinates in this ROI. The details are shown in Table 1.

Table 1 UAV target location method based on cascaded deep learning models.

UAV target location method based on cascaded deep learning models

Input：
  Captured images I
  PTU attitudes (yaw, $pitch$)
  UAV dataset with labels M
Output：UAV localization coordinates (x, y, z)
BL-Net and PR-Net Training Procedure：
for *batch* in M:
  for X_i in *batch*:
    a) Obtain the *BboxLocate-Net* image label：Category C and Bbox coordinate (x, y, w, h), *PointRefine-Net* image label：key point coordinate (x, y)
    b) Initializing Network parameters and forward propagation.
    while X_i = true do:
      if $Loss$ >= T:
        a) Backward propagation
        b) Gradient descent with momentum
        c) Forward propagation, get *Loss* value
      else: Save model: obtain the *BL-N* and *PR-N*
    end
  end
end
Test Procedure：
Step 1: *BboxLocate-Net* image object detection;
  a) Resize the captured image resolution to (320,240)
  b) Forward propagation: predict Bbox coordinate (x, y, w, h)
  c) Suppression Bbox of $t_0 < 0.6$
  d) Non-maximum Suppression
  e) Object detection result：Bbox center (u, v)
Step 2: EKF-based object spatial localization algorithm and Motion continuity judgment;
  a) Get positioning result (x, y, z) from（u, v）and PTU attitudes (yaw, $pitch$)
  b) Motion continuity judgment:
    if (x, y, z) is a wrong point：
      Go to Step 3：*PointRefine-Net* receives the key ROI (x, y, w, h)；
    else:
      Return the final positioning value (x, y, z)
Step 3: *PointRefine-Net* image key point detection;
  a) Resize the captured image resolution to (30, 30)
  b) Forward propagation: predict key point coordinate (u, v)
  c) Get positioning result (x, y, z) with EKF-based localization algorithm and Return (x, y, z).

4. Cascaded deep learning model-based detection experiment

Aiming at the performance evaluation of the novel target detection method proposed in this paper, we carry on the contrast analysis between the image detection performance and the real-scenario flight trajectory solution. In the image target detection experiment, the experimental data comes from a large number of UAV landing mixed images generated by actual and simulation flight experiments. We design the following two groups of experiments to compare the cascade deep learning model with other classical detection algorithms in terms of real-time and accuracy performance.

(1) The first experiment verifies the accuracy and real-time performance of *BboxLocate-Net* by comparing it with several classical deep learning target detection algorithms.

(2) The second experiment analyses the detection accuracy of *PointRefine-Net* and *BboxLocate-Net*, and proves that the second level network has certain optimization ability for the results detected by first level network.

4.1. Dataset and Evaluation Protocol

In this study, we train *BboxLocate-Net* network based on open source framework Darknet and *PointRefine-Net* on Caffe. The testing facility is a PC device with an internal storage 64GB and an operating system Ubuntu 14.04; CPU is i7-5930K, and GPU is NVIDIA GeForce GTX 1080ti.

Our previous research has successfully carried out several experiments under good weather conditions.[3,9,13] For meeting the needs of deep learning, we present an upgraded version of our self-constructed dataset which includes images from our previous dataset and new extracted images captured in the simulation system. Our new dataset not only contained a larger number of images but also was gathered in more challenging weather conditions (stronger wind smog and heavy snow). The UAV position can also be set up in the distance and attitudes to expand the diversity of data samples. The dataset used in the experiment is an integration of simulated and actual datasets, of which the mixed train dataset consists of actual train dataset and simulated dataset, totaling 13,350 pictures. And the mixed validation dataset includes the actual validation dataset and the simulation validation dataset, with a total of 1500 pictures. For real-scenario flight application, we only test our algorithm on the actual flight dataset.

In this section, four evaluation indexes are adopted for evaluating cascade deep learning networks. We use mean average precision (mAP) and frames per second (FPS) to evaluate the proposed *BboxLocate-Net* model. And the performance of *PointRefine-Net* is measured with the average detection error - "Mean Error" and the failure rate of each key point - "False Rate".

The above mentioned two evaluation indexes mAP and FPS both have clear meanings in the target detection field. We won't define them here. The Mean error defined in this paper is measured as:

$$MeanError = \frac{\|(u,v)-(\hat{u},\hat{v})\|}{BBox.w} \times 100\% \tag{12}$$

where (u, v) and $(\hat{u},\hat{v})$ are the ground truth and the detected position. $BBox._w$ is the width of the bounding box detected by *BboxLocate-Net*.

In order to evaluate the accuracy of network prediction results, we define another indicator: False Rate. For the key point detection result of each frame, if the error is larger than 5%, it is considered the detection result of this frame as a failure. This means that the key point position error in each direction cannot be greater than 5% of the target area. In a group of experiments, the key point detection accuracy is defined as the ratio of the number of key points detected failure to the total number of key points.

4.2. BboxLocate-Net model-based detection experiments

High precision target detection in image is the foundation of high accuracy positioning in stereo vision system. At the same time, the real-time performance of the detection algorithm is also the key factor for the system to be practical.

To make a fair comparison between *BboxLocate-Net* and other algorithms in real time and accuracy, we have trained all kinds of deep learning methods[20,28,29,30] under the same conditions. Table 2 summarizes the training parameters we used on training the UAV detection model. The training details of the network are as follows.

Table 2 Table of training parameters of five deep learning algorithms.

	BboxLocate-Net	**YOLO V3**	**YOLO V3-Tiny**	**YOLO V2-Tiny**	**MobileNet-YOLO**
Input size (unit: px)	320×240	320×240	320×240	320×240	320×240
Number of epochs	150000	150000	150000	150000	150000
Batch size	64	64	64	64	64
Initial Learning rate	0.0001	0.0001	0.0001	0.0001	0.0001
Momentum	0.9	0.9	0.9	0.9	0.9
Decay	0.0005	0.0005	0.0005	0.0005	0.0005
Backbone	BboxLocate-Net	Darknet-53	Darknet-21	Darknet-19	Mobilenets v1

The initialization of *PointRefine-Net* parameters is the same as that of *BboxLocate-Net*. Its input image resolution is *30×30*, and the batch size is set to 32. We also use small batch random gradient descent to optimize network parameters. The network trained about 150000 times in total, and stopped training when the loss value was less than 0.002.

Using mixed landing dataset, we compared the proposed *BboxLocate-Net* detection results with that obtained by state-of-the-art CNN object detectors such as MobileNets-SSD[29,30], YOLO V2-Tiny[28], YOLO V3-Tiny[20] and MobileNets-YOLO[20,29]. We use mAP and FPS as comparison indicators for these algorithms. The performance comparison of our algorithm and the existing state-of-the-art approaches is shown in Table 3. Our approach is significantly better than MobileNets-SSD and YOLO V2-tiny approaches. On the other hand, our tiny network, *BboxLocate-Net*, achieves an AP of 0.963 and FPS of 503. It outperforms most other algorithms, and is more efficient in terms of model size and computation complexity (GFLOPs). Fig.5 shows the partial detection results of different CNN detection algorithms.

Table 3 The Comparison of mAP value and FPS at IoU = 0.5 of different CNN detectors.

Algorithms	Sunny			Rain			Snow			Entire Dataset	FPS
	8:00	12:00	17:00	8:00	12:00	17:00	8:00	12:00	17:00		
BboxLocate-Net	0.96	0.97	0.95	0.96	0.98	0.98	0.97	0.96	0.93	0.963	503
YOLO V3	0.98	0.97	0.94	0.98	0.97	0.95	0.97	0.98	0.95	0.966	31.89
YOLO V3-Tiny	0.93	0.94	0.95	0.91	0.94	0.92	0.94	0.95	0.91	0.932	221
YOLO V2-Tiny	0.91	0.90	0.89	0.89	0.93	0.91	0.92	0.94	0.90	0.910	230
MobileNets-SSD	0.91	0.93	0.92	0.94	0.91	0.92	0.89	0.91	0.94	0.919	289
MobileNets-YOLO	0.89	0.91	0.89	0.91	0.94	0.91	0.92	0.93	0.94	0.916	291

Fig. 5. The test results of different CNN algorithms.

4.3. PointRefine-Net model-based detection experiments

For the performance analysis of *PointRefine-net* network, we take Mean Error and False Rate as evaluation indexes. In order to test the key point positioning effect in the algorithm, we synthetically analyzed the positioning results of six UAV key points and compared the detection results before and after *PointRefine-Net.* Fig.6 shows the comparison of the Mean Error and False Rate between *PointRefine-Net* and *BboxLocate-Net* when detecting six key points. Compared with *BboxLocate-Net*, the detection results of *PointRefine-Net* have improved the accuracy to some extent and can be used as a correcting network for error points. Fig.7 shows the comparison of several detection results before and after *PointRefine-Net* correction.

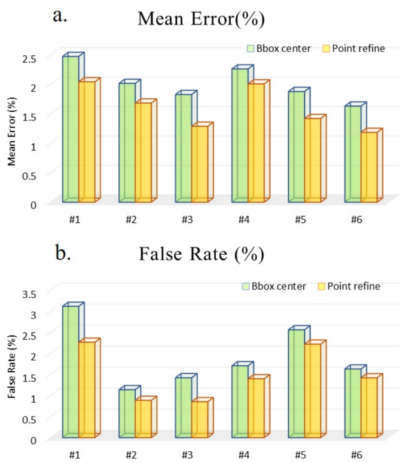

Fig. 6. Comparison of detection results at 6 key points before and after coordinate correction (a) Mean Error; (b) False Rate

Fig. 7. Comparison of key point detection results before and after the coordinates correction.

5. Real-scenario flight localization experiments

The real-scenario flight localization experiments are based on the ground-based visual system mentioned above. The runway baseline is about 10.77 meters. The high precision PTU is set on both sides of the runway and a DFK 23G445 camera is fixed on the PTU. Each of PTU has two degree of freedom to expand the search field. At the same time, the high position resolution (0.00625 degrees) and high rotation speed (50 degrees/second) make a higher positioning accuracy. The target detection method mentioned in the paper is used to process the images collected by the two cameras, and then the positioning results are compared with the previous work.

To comprehensively verify the performance of our algorithm in real-scenario flight, we take the cascaded deep learning detection algorithm proposed in this paper and EKF-based localization algorithm[3] as the solution algorithm, and design the following two groups of flight experiment.

(1) The first group is based on Chan-Vese algorithm, GOTURN algorithm and *Bboxlocate-net* algorithm to calculate the UAV space trajectory, and to compare the accuracy and real-time capacity.

(2) To prove the better accuracy and robustness of the system after the *PointRefine-Net* coordinate correction algorithm, the second group mainly compares the influence of *PointRefine-Net* coordinate correction algorithm and *Bboxlocate-net* algorithm on the accuracy and robustness capacity.

5.1. BboxLocate-Net model-based localization experiments

(1) Experiment 1.1: Accuracy experiments without *PointRefine-Net*

Fig.8 shows autonomous landing trajectories and localization errors in X, Y and Z directions. One trajectory is calculated by EKF-based localization algorithm. The blue trajectory is generated by DGPS as a reference trajectory, and the yellow, light blue and red ones are generated by Chan-Vese, GOTURN and *BboxLocate-Net* algorithms, respectively.[3,13] The blue area, green area and yellow area in Fig.9 represent three stages of approaching, descending and taxiing in the landing process. The root-mean-square error (RMSE) in each axis using EKF is presented in the right of the Fig.9.

According to Fig.9, the *BboxLocate-Net* localization algorithm reduces the deviation to some extent at all three axes, especially in the "Air&Ground" stage, the trajectory generated by *BboxLocate-Net* has a smaller deviation than that of Chan-Vese and GOTURN algorithm, which shows a significant improvement to autonomous landing. In conclusion, the localization accuracy improvement brought by *BboxLocate-Net* localization algorithm shows greater significance to UAV autonomous landing.

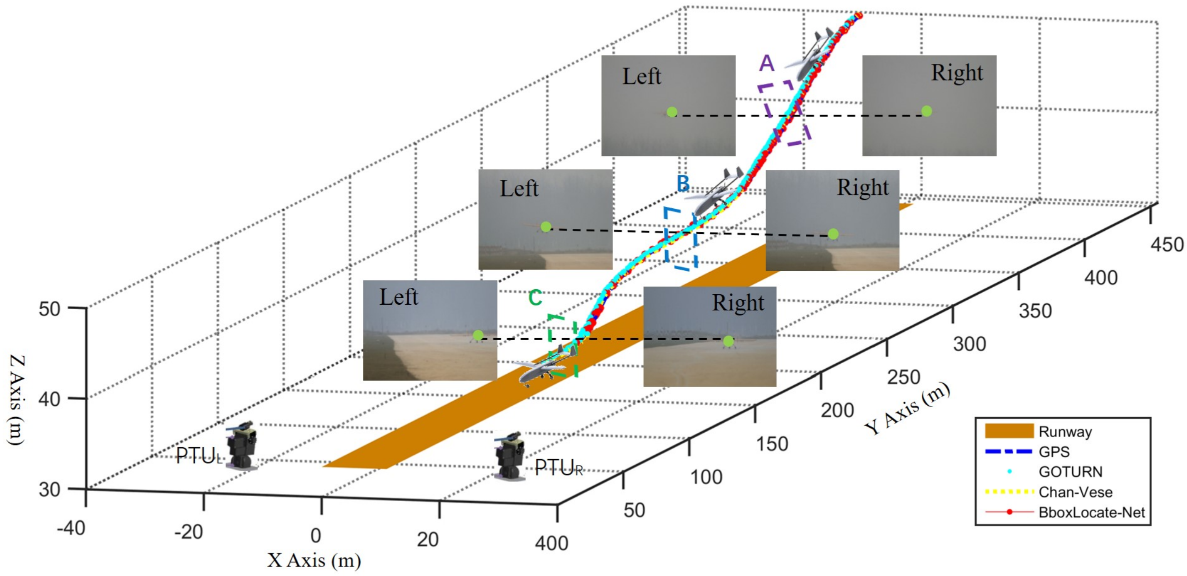

Fig. 8. Localization results using different UAV detection algorithm. The blue trajectory is the reference trajectory generated by DGPS. The yellow, light blue and red trajectories are generated by Chan-Vese, GOTURN and *BboxLocate-Net* detection algorithm and EKF-based localization algorithm, respectively. The Y global axis is along with the direction of the runway.

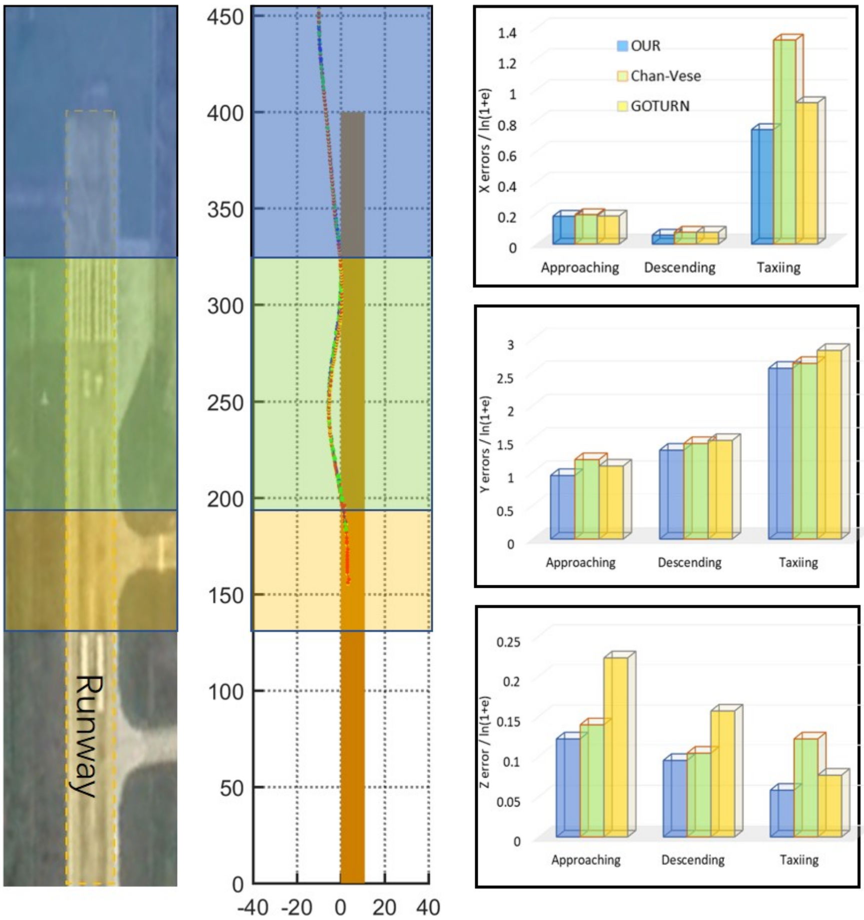

Fig. 9. Accuracy comparison of spatial positioning results. For the convenience of display, the error is displayed after taking *ln*(*1*+*e*). Comparison among Chan-Vese, GOTURN and *BboxLocate-Net*. The blue, green and yellow area on the left side of the picture respectively represent approaching, descending, taxiing stages.

(2) Experiment 1.2: Real-time capability experiments without *PointRefine-Net*

The real-time performance of the algorithm has always been a key and common problem in practical engineering applications, and it is also our focus.

We compare the frames per second (FPS) of object detection with different algorithms, and these algorithms are tested in the same equipment, which is a PC with i7-5930K CPU and 64 GB internal storage. The results are shown in Table 4. The detection speed of *BboxLocate-Net* can reach 500fps, about 500 times of Chan-Vese algorithm and 3 times of GOTURN algorithm. Compared with Chan-Vese algorithm and GOTURN algorithm, our method has great progress in real-time capability.

Table 4 RMSE with EKF at each axis of the actual landing experiments and FPS using three different detection methods.

Index	Algorithm	X(m)	Y(m)	Z(m)	FPS
T1	Chan-Vese	0.3205	2.8605	0.1530	10.23±0.8
	GOTURN	0.3387	2.9821	0.1324	172.56±2.42
	BboxLocate-Net	0.3107	2.6782	0.1203	500.23±2.21

5.2. Cascaded deep learning model-based localiza tion experiments

(1) Experiment 2.1: Robustness capability experiments with *PointRefine-Net*

Another trajectory is shown in Fig.10. The image detection results at point D and F with large deviation in Fig.10 are shown in Fig.11 (a) and (b). It shows that the location error is mainly caused by the wrong image detection results. We conduct *PointRefine-Net* operation at point D and F. The light blue dot and yellow dot are the results before and after correction, respectively. And the light blue trajectory and yellow trajectory in Fig.11 respectively represent the positioning results before and after correction. We can see that *PointRefine-Net* shows better robustness than *BboxLocate-Net* algorithm.

In Fig.10, the S area represents the case that part of the UAV goes out of the field of view. The detection results of four typical frames in S area are shown in Fig.12, Purple points are the detection results of Chan Vese, red points indicate the detection results of GOTURN, light blue and yellow points indicate the detection results before and after *PointRefine-Net* network respectively. When the target image coordinates out of the FOV, the comparison of detection results also shows that *PointRefine-Net* has a more robust performance.

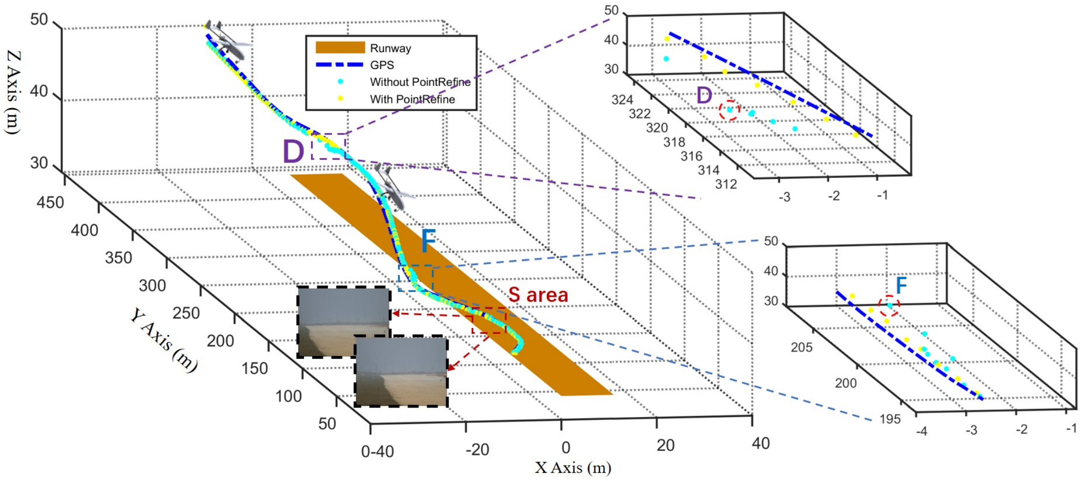

Fig. 10. Comparison of localization results before and after *PointRefine-Net*. In the figure, D and F are the two points with large error. The S area represents the case that part of the UAV target is outside the FOV.

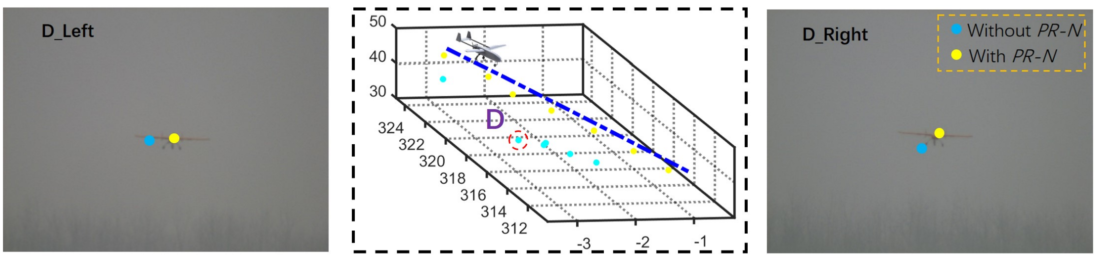

(a) Left image and right image at point D.

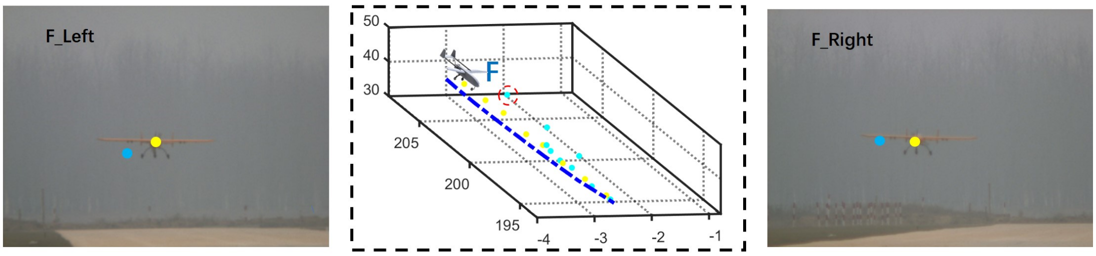

(b) Left image and right image at point F.

Fig. 11. Comparison of key point detection results before and after *PointRefine-Net* (*PR-N*) coordinate correction. (a) The detection results at D point; (b) The detection results at F point.

Fig. 12. The key point detection results detected by four detection algorithms. G, H, I and J represent four typical frames out of the FOV in the S area.

(2) Experiment 2.2: Accuracy experiments with *PointRefine-Net*

The light blue and yellow trajectories in Fig.10 are generated by different detection algorithms but same localization algorithms. Same as above, Blue is generated by DGPS, and light blue and yellow are generated by *BboxLocate-Net* and *PointRefine-Net* algorithm, respectively. Table 5 shows the comparison of RMSE with EKF at each axis between the two algorithms in actual landing experiments. It can be seen that the algorithm after *PointRefine-Net* has higher location accuracy.

(3) Experiment 2.3: Real-time capability experiments with *PointRefine-Net*

We use the flight trajectory mentioned in experiment 2.1 to compare the location speed before and after *PointRefine-Net*. The results are shown in Table 5. *BboxLocate-Net* algorithm has better real-time capability, but *PointRefine-Net* algorithm has higher location accuracy while the real-time capability is kept in the same level.

Table 5 RMSE with EKF at each axis of the actual landing experiments and FPS before and after *PointRefine-Net*. BL-N and PR-N denote the *BboxLocate-Net* and *PointRefine-Net*, respectively.

Index	Algorithm	X(m)	Y(m)	Z(m)	FPS
T2	BL-N without PR-N	0.2456	1.8082	0.1213	500.23±2.21
	BL-N with PR-N	0.2323	1.6002	0.1156	450.32±2.34

6. Concluding remarks

In this paper, a novel cascaded deep learning detection models has been proposed and developed for autonomous landing of unmanned fixed-wing aerial vehicles. A light-weight deep learning model enables a higher processing speed and makes the reasonable check and further optimization of UAV coordinates a reality. Flight experiment results validate that the approach attaches ~500 fps and higher positioning accuracy than previous work. By making full use of the expansibility of the ground computing resources, we promote the visual guidance landing system to be practical.

In the subsequent work, the developed algorithm is potentially extended to enabling detection and localization based on multiple key areas and key points. This algorithm is also to be developed from vision-based position to pose (position-and-attitude) during the autolanding. In details, multiple anchors are to be detected simultaneously to support pose estimation then.

References

1. Kumar V, Michael N. Opportunities and challenges with autonomous micro aerial vehicles. The International Journal of Robotics Research 2012; 31(11):1279-91.
2. Kendoul F. Survey of advances in guidance, navigation, and control of unmanned rotorcraft systems. Journal of Field Robotics 2012; 29(2):315-78.
3. Tang D, Hu T, Shen L, Zhang D, Kong W, Low KH. Ground stereo vision-based navigation for autonomous take-off and landing of UAVs: A Chan-Vese model approach. International Journal of Advanced Robotic Systems 2016; 13(2):67.
4. Gui Y, Guo P, Zhang H, et al. Airborne vision-based navigation method for UAV accuracy landing using infrared lamps. Journal of Intelligent & Robotic Systems 2013; 72(2):197-218.
5. Bourquardez O, Chaumette F. Visual servoing of an airplane for auto-landing. 2007 IEEE/RSJ International Conference on Intelligent Robots and Systems. 2007; 1314-9.
6. Pebrianti D, Kendoul F, Azrad S, Wang W, Nonami K. Autonomous hovering and landing of a quad-rotor micro aerial vehicle by means of on ground stereo vision system. Journal of System Design and Dynamics 2010; 4(2):269-84.
7. Yang T, Li G, Li J, et al. A ground-based near infrared camera array system for UAV auto-landing in GPS-denied environment. Sensors 2016; 16(9):1393.
8. Santos NP, Lobo V, Bernardino A. AUTOLAND project: Fixed-wing UAV Landing on a Fast Patrol Boat using Computer Vision. OCEANS 2019 MTS/IEEE SEATTLE. 2019; 1-5.
9. Kong W, Zhang D, Wang X, Xian Z, Zhang J. Autonomous landing of an UAV with a ground-based actuated infrared stereo vision system. 2013 IEEE/RSJ International Conference on Intelligent Robots and Systems. 2013; 2963-70
10. Guan B, Sun X, Shang Y, Zhang X, Hofer M. Multi-camera networks for motion parameter estimation of an aircraft. International Journal of Advanced Robotic Systems 2017; 14(1):1729881417692312.
11. Hu T, Zhao B, Tang D, Zhang D, Kong W, Shen L. ROS-based ground stereo vision detection: Implementation and experiments. Robotics and biomimetics 2016; 3(1):14.
12. Ma Z, Hu T, Shen L. Stereo vision guiding for the autonomous landing of fixed-wing UAVs: a saliency-inspired approach. International Journal of Advanced Robotic Systems 2016; 13(2):43.
13. Cao Z, Zhao K, Fang Q, Kong W, Tang D, Hu T.

Enabling~ 100fps detection on a landing unmanned aircraft for its on-ground vision-based recovery. 2017 18th International Conference on Advanced Robotics (ICAR). 2017; 407-11.

14. Tang D, Hu T, Shen L, Zhang D, Zhou D. Chan-Vese model based binocular visual object extraction for UAV autonomous take-off and landing. 2015 5th International Conference on Information Science and Technology (ICIST). 2015; 67-73.
15. Kong W, Zhou D, Zhang Y, et al. A ground-based optical system for autonomous landing of a fixed wing UAV. 2014 IEEE/RSJ International Conference on Intelligent Robots and Systems. 2014; 4797-804.
16. Daibing Z, Xun W, Weiwei K. Autonomous control of running takeoff and landing for a fixed-wing unmanned aerial vehicle. 2012 12th International Conference on Control Automation Robotics & Vision (ICARCV). 2012; 990-4.
17. Chengping Y, Lincheng S, Dianle Z, Daibing Z, Zhiwei Z. A new calibration method for vision system using differential GPS. 2014 13th International Conference on Control Automation Robotics & Vision (ICARCV). 2014; 1514-7.
18. Zhang Y, Shen L, Cong Y, Zhou D, Zhang D. Ground-based visual guidance in autonomous UAV landing. Sixth International Conference on Machine Vision (ICMV 2013). 2013; 90671W.
19. Ren S, He K, Girshick R, Sun J. Faster r-cnn: Towards real-time object detection with region proposal networks. Advances in neural information processing systems. 2015; 91-9.
20. Redmon J, Farhadi A. Yolov3: An incremental improvement. arXiv preprint arXiv:180402767 2018.
21. Huang G, Liu Z, Van Der Maaten L, Weinberger KQ. Densely connected convolutional networks. Proceedings of the IEEE conference on computer vision and pattern recognition. 2017; 4700-8.
22. Sun K, Xiao B, Liu D, Wang J. Deep high-resolution representation learning for human pose estimation. Proceedings of the IEEE Conference on Computer Vision and Pattern Recognition. 2019; 5693-703.
23. Lin T-Y, Maire M, Belongie S, et al. Microsoft coco: Common objects in context. European conference on computer vision. 2014; 740-55.
24. Deng J, Dong W, Socher R, Li L-J, Li K, Fei-Fei L. Imagenet: A large-scale hierarchical image database. 2009 IEEE conference on computer vision and pattern recognition. 2009; 248-55.
25. Tang X, Yang W, Hu X, Zhang D. A novel simplified model for torsional vibration analysis of a series-parallel hybrid electric vehicle. Mechanical Systems and Signal Processing 2017; 85:329-38.
26. Newell A, Yang K, Deng J. Stacked hourglass networks for human pose estimation. European conference on computer vision. 2016; 483-99.
27. Everingham M, Van Gool L, Williams CK, Winn J, Zisserman A. The pascal visual object classes (voc) challenge. International journal of computer vision 2010; 88(2):303-38.
28. Redmon J, Farhadi A. YOLO9000: better, faster, stronger. Proceedings of the IEEE conference on computer vision and pattern recognition. 2017; 7263-71.
29. Howard AG, Zhu M, Chen B, et al. Mobilenets: Efficient convolutional neural networks for mobile vision applications. arXiv preprint arXiv:170404861 2017.
30. Liu W, Anguelov D, Erhan D, et al. Ssd: Single shot multibox detector. European conference on computer vision. 2016; 21-37.